Aerosol and Air Quality Research, 18: 866–883, 2018

ISSN: 1680-8584 print / 2071-1409 online
doi: 10.4209/aaqr.2018.02.0058

Flow Dynamics and $PM_{2.5}$ Deposition in Healthy and Asthmatic Airways at Different Inhalation Statuses

Wei-Hsin Chen[1,2*], Kuo-Hao Lee[1], Justus Kavita Mutuku[3], Chii-Jong Hwang[1]

[1] *Department of Aeronautics and Astronautics, National Cheng Kung University, Tainan 70101, Taiwan*
[2] *Research Center for Energy Technology and Strategy, National Cheng Kung University, Tainan 70101, Taiwan*
[3] *Department of Environmental Engineering, National Cheng Kung University, Tainan 70101, Taiwan*

ABSTRACT

Public health reports indicate that high $PM_{2.5}$ concentration can impair the respiratory health of the residents, especially for those affected by asthma. Therefore, there is a need to determine the deposition mechanism and efficiencies for $PM_{2.5}$ in asthmatic human airways. In this study, gas flow dynamics and deposition fractions (DFs) of $PM_{2.5}$ in generations 10–11 of Weibel's lung model were investigated where the two-phase gas-solid flow behaviors in healthy and asthmatic airways were considered. The gas phase was modeled as a transient laminar and incompressible flow while the discrete phase model (DPM) was applied for the particle phase. Three different air flow rates under rest, light activity, and moderate exercise were considered. For the healthy airways, higher total mass DFs were observed during a moderate exercise as compared to rest and light activity conditions. Deposition fractions were higher in asthmatic airways compared to those of healthy ones, stemming from tapering in the airways as well as complex secondary flow fields, namely, Dean vortices, in the folds. Deposition was mainly due to inertial forces of particles, but a small amount of $PM_{2.5}$ was deposited near the entrance of asthmatic tube, as a result of the secondary flow. The numerical results revealed that the Dean vortices was an important factor for particle deposition. With increased DF, asthmatic people have a higher total respiratory dose of $PM_{2.5}$ for a given exposure compared to healthy individuals. Thus contributing to their increased susceptibility to adverse health effects caused by $PM_{2.5}$.

Keywords: $PM_{2.5}$; Airway and asthma; Transient flow and inhalation; Two-phase flow; Computational fluid dynamics (CFD).

NOMENCLATURE

A	Amplitude of the sinusoidal curve (Reynolds number)
A_{fold}	Amplitude of the folds (cm)
A_0	Cross- sectional area of the lumen (cm^2)
C	Concentration (cm^{-3})
C_D	Drag coefficient
DF	Deposition fraction
D	Diameter (mm)
d_p	Particle diameter (μm)
F	Force (N)
G	Generation of Weibel's airway
m_p	Mass of a single particle (μg)
n	Number of folds
P	Pressure (pa)
Q	Flow rate (L s^{-1})
R	Radius (mm)
r	Radial coordinate
Re	Reynolds number
t	Time (s)
u_p	Particle velocity (m s^{-1})
Umean	Average velocity at the airway's entrance (m s^{-1})
U_{max}	Max velocity at the airway's entrance (m s^{-1})
V	Control volume

Greek Letters

ρ	Density (kg m^{-3})
σ	Stress (N m^{-2})
μ	Viscosity Coefficient
α_f	Fluid volume fraction
θ	Angular coordinate (°)

Subscripts

p	particle
mean	average value
peak	peak value

*Corresponding author.
E-mail address: chenwh@mail.ncku.edu.tw; weihsinchen@gmail.com

INTRODUCTION

Among the particles found suspended in the ambient air, $PM_{2.5}$ is one of the most harmful particles to humans (Donaldson *et al.*, 2001; Zheng *et al.*, 2016b). The side effects of $PM_{2.5}$ to the human body include airway damages, cardiovascular impairments, exacerbation of diabetes mellitus, and adverse effects to infants (Feng *et al.*, 2016; Xing *et al.*, 2017). Asthma and chronic obstructive pulmonary disorder (COPD) are some of the conditions which come as a result of deformations of human airways. Asthma occurs as a result of chronic inflammation of airways, especially on small bronchioles, which leads to increased contractibility of the surrounding smooth muscles (Macklem, 1996). Since the walls in asthmatic airways are significantly thickened, the airway obstruction results in breathing difficulties (Jain *et al.*, 2013). Studies had shown that elevated levels of $PM_{2.5}$ and rhinovirus infection could exacerbate asthma (Vempilly *et al.*, 2013; Tang *et al.*, 2017). Large amounts of suspended particles could lower the pH value in a patient suffering from acute asthma, due to an increase in hydrogen ions (McCreanor *et al.*, 2007). Low pH values in turn reduce the hemoglobin's affinity for oxygen in the lungs.

The main sources of particulate matters are composite particle phase and gas phase emitted from cooking fumes and road dust (Schauer *et al.*, 2002; Lee *et al.*, 2016). Analysis of $PM_{2.5}$ also shows organic matters, indicating a noticeable contributions from gasoline-powered motor vehicle exhaust, diesel engine exhaust, meat cooking, and photochemical smog. Major sources of atmospheric fine particles are associated with modern industrialization. The main chemical compounds in the particulate matters collected from the southern part of Taiwan were sulfate, nitrate, and carbon (Lin *et al.*, 2008; Tsai *et al.*, 2011). An analysis by Kuo *et al.* (2007) indicated that arsenic, selenium, cadmium, antimony, and mercury were the main metallic elements in $PM_{2.5}$ found in Tainan, Taiwan. The sources of this $PM_{2.5}$ were mainly coal combustion, waste incineration, and construction works. In order to investigate the flow properties of fine suspended particles, the density of the particles was required (Kannosto *et al.*, 2008; Zheng *et al.*, 2016a). Atmospheric particles were usually assumed to have a spherical shape with a bulk density ranging from 1.1 to 2 g cm^{-3}, and the measurements were carried out using a scanning mobility particle sizer (SMPS) (Khlystov *et al.*, 2004; Liu *et al.*, 2015). In practice, particulate matter usually has amorphous, spherical, and irregular shapes; however, most of the particles are smooth and spherical (Wang *et al.*, 2017a; Wang *et al.*, 2017b). In a study done in Pittsburgh by Rees *et al.* (2004), the effective particle density was found to be 1.5 ± 0.3 g cm^{-3}. Another study done in Beijing China by He *et al.* (2001), found that the average density during summer was 1.6 ± 0.43 g cm^{-3}, while during winter it was 1.41 ± 0.40 g cm^{-3}. Morawska *et al.* (1999) studied the relationship between the total number of sub micrometer airborne particles and the volume concentrations using SMPS, and the estimated average density of the sub micrometer particles was found to be between 1.2 and 1.8 g cm^{-3}. The latest study on the relationship between $PM_{2.5}$ concentration and size distribution within the urban areas of Taiwan was done by Chen *et al.* (1997).

Earlier simulation of particle flow in the human airways assumed a parabolic distribution at the inlet. This distribution has showed a good agreement in the comparison between the deposition rates from laboratory experiments and numerical analysis (Kim and Iglesias, 1989; Zhang *et al.*, 1997). Therefore, in this study, a deterministic-parabolic distribution of particles at the inlet was assumed. A "trap upon impact" boundary condition was imposed on all airway walls due to the mucus found on the surface of tracheobronchial airways (Nazridoust and Asgharian, 2008). The numerical results revealed that the secondary flows in the asthmatic airway bifurcation were much stronger than in the healthy one, resulting in higher particle deposition. The sinusoidal folds were responsible for the blocking phenomenon which mainly occurred in the small airways (Ebina *et al.*, 1990).

In an earlier study by Zhang and Papadakis (2010) about particle deposition in an asthmatic human airway, a steady flow was investigated numerically. The results showed that deposition in an asthmatic airway was higher compared to a healthy one due to the secondary velocities caused by the folds. However, to the authors' knowledge, investigations on airflow and particle deposition patterns in asthmatic human airways under three different transient breathing conditions have not been performed yet. Over the past several decades, computational fluid dynamics (CFD) has become an important tool to predict aerosol physics (Chen, 2001a, b; Chen *et al.*, 2011, 2014). For these reasons, $PM_{2.5}$ deposition in generations 10 and 11 (G10 and G11) under the transient breathing conditions and the Weibel's airway model for healthy and asthmatic airways were investigated numerically in this study. Air containing a $PM_{2.5}$ concentration of 50 μg m^{-3} during transient inhalation was injected into asthmatic and healthy airways. It has been shown that air flow pattern and particle's sizes had an impact on the deposition pattern in the human airways (Donovan and Tawhai, 2010; Huang and Zhang, 2011). Therefore, four different particle sizes and three different breathing conditions were considered. The effects of air flow velocities, particle size, and bifurcation configuration on particle deposition were evaluated. The findings are useful in terms of setting up limits of $PM_{2.5}$ for patients with deformed airways, especially for those suffering from asthma.

MATHEMATICAL FORMULATION

Model Geometry

Several studies have been done on the lung's geometry, and there are two main ones. The Weibel's geometry assumes a symmetrical geometry, while the Horsfield's model assumes an asymmetrical structure (Weibel, 1963b; Horsfield *et al.*, 1971). Results obtained from a study on the deposition rates from the two models showed that the deposition fractions in the Weibel's model were slightly higher than those in the Horsfield's model. The Weibel's

model was used as the basis for this study because it is simple and its simulation requires less computational effort and time. Accordingly, three-dimensional solid models and grid systems of generations 10 and 11 (G10 and G11) of healthy and asthmatic airways were constructed to stand for the symmetrical bronchial models, as shown in Figs. 1(a) and 1(b), while the geometric parameters are provided in Table 1. The healthy model had both G10 and G11 with smooth airways, whereas the second model was composed of a healthy G10 and asthmatic G11. The tubular models of the human G10 and G11 airways were established according to the Weibel's 23-generation pulmonary model with a bifurcation angle of 60° (Weibel, 1963a). The airway geometry was rigid and symmetric with respect to the plane z = 0 and the y-axis.

The geometry of the asthmatic human airway can be represented by a circular cross-section with sinusoidal waves to represent the epithelial tissue folds (Lambert *et al.*, 1994; Wiggs *et al.*, 1997). The epithelial folds reduce the volume of the airways. The smooth muscles further constrict, causing buckling of the mucous layer and thus reducing the volume even further. Analytical and finite element methods have been applied to investigate the onset of buckling of an asthmatic airway cross-section (Hrousis *et al.*, 2002). According to a study on the tracheal changes in terms of the elastic properties of the airways due to mucosal folding, the nature of the folds and the resistance to flow were the functions of the configuration of asthmatic airways (Donovan and Tawhai, 2010). According to the study of Zhang and Papadakis (2010), an asthmatic airway could be represented as a circular cross-section surrounded by a number of sinusoidal folds which are distributed along the circumference. Mathematically, it is expressed in the polar coordinate system as:

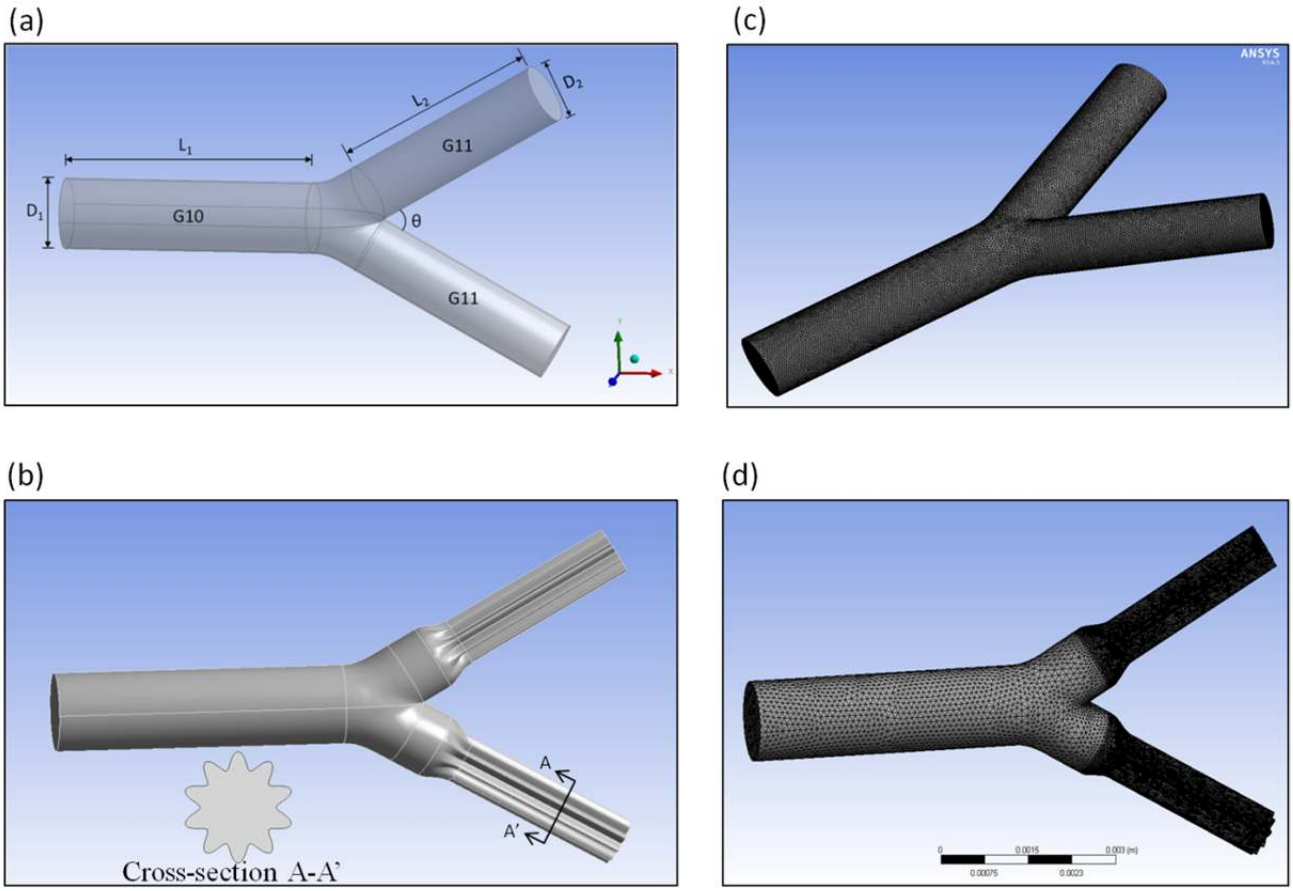

Fig. 1. Three-dimensional solid model of generations 10–11 where (a) G10 and G11 are healthy and (b) G10 is healthy while G11 is asthmatic, and schematics of grid system where (c) G10 and G11 are healthy and (d) G10 is healthy while the two G11 are asthmatic airways.

Table 1. Geometric parameters of the bifurcation model.

Parameter	Generation number			
	10		11	
Length L_i (mm)	L_1	1.29	L_2	1.10
Diameter D_i (mm)	D_1	4.57	D_2	3.85
Bifurcation angle (°)	-		30	

$$r(\theta) = R + A_{fold}\, cos(n\theta) \quad (1)$$

where r is the radial coordinate, θ is the angular coordinate, R is the effective radius of cross-section, A_{fold} is the fold's amplitude in centimeters, and n is the number of folds in the cross-section. In this study, the computational domain of the asthmatic airway is discretized with 40% of normal lumen area (= 0.40A0) and 10 folds (i.e., n = 10) (Fig. 1(b)).

Governing Equations

The gas flow fields and deposition patterns during inhalation were simulated, based on the assumptions of isothermal, incompressible, and laminar flow, smooth and rigid airways, and no-slip on the airway walls. Constant kinematic viscosity (μ) and density (ρ) were also assumed, while the effect of gravity was negligible. The gravitational force affects particles when their diameters are larger than 10 μm (Hofmann *et al.*, 1995). The present study focused on particles smaller than 2.5 μm. Therefore, the effect of gravity on particles was ignored. The conservation equations for a gas-solid two phase flow are written as follows (Johnson and Jackson, 1987; Morel, 2015).

Continuity equation:

$$\frac{\partial}{\partial x_i}\left(\alpha_f U_i\right) = 0, \quad i = 1,2,3 \quad (2)$$

Momentum equation:

$$\frac{\partial}{\partial t}\left(\alpha_f U_i\right) + \frac{\partial}{\partial x_j}\left(\alpha_f U_j U_i\right) = -\frac{\alpha_f}{\rho}\frac{\partial P}{\partial x_i} + \frac{\partial}{\partial x_j}\left(\alpha_f \sigma_{ij}\right) + F_{pf}, \quad i = 1,2,3 \text{ and } j = 1,2,3 \quad (3)$$

In the preceding equations, x_i represents Cartesian coordinates, t is the elapsed time, U_i and P designate the local airflow velocity and pressure, respectively, ρ is the air density, σ_{ij} is the shear stress wherein the subscripts i and j stand for y and z coordinates, respectively, and F_{pf} represents viscous forces on the particles.

Considering a particle's motion, it is governed by Newton's second law of motion which is expressed as

$$m_p \frac{du_p}{dt} = F_{fp} \quad (4)$$

This implies, in turn, that the particle trajectory is described by the following equation, without considering external force, temperature change, and magnetic field (Feng and Kleinstreuer, 2014).

$$m_p \frac{du_p}{dt} = \frac{1}{8}\pi \pi_p^{\,2} \rho C_D \left(u - u_p\right)\left|u - u_p\right| = F_{fp} \quad (5)$$

In this equation, m_p is a single particle mass, and d_p and u_p are the particle diameter and velocity, respectively. The particles were assumed to be spherical, and their motions were affected by their inertial forces and fluid flows inside the airways. $PM_{2.5}$ disintegrates only under extreme environmental conditions such as high temperatures and pressure which don't usually occur in the natural ambient environment (Zhang *et al.*, 2016). Therefore, the particles were also assumed to neither break nor deform from the rotational movement inside the airways. The drag coefficient C_d is defined as

$$C_d = \alpha_1 + \frac{\alpha_2}{Re_N} + \frac{\alpha_3}{Re_N^{\,2}} \quad (6)$$

where α_1, α_2, and α_3 are the coefficients determined by the Reynolds number (Re_N) (Morsi and Alexander, 1972). The Reynolds number of a spherical particle is written as

$$Re_N = \frac{\rho\left|v - v_p\right| D_p}{\mu} \quad (7)$$

The difference between a gas-solid two-phase flow and a single phase flow was represented by the fluid volume fraction (α_f), which referred to the proportion of gas in the volume occupied by the control volume, i.e., $\alpha_f = 1$ for a continuous phase:

$$\alpha_f = 1 - \frac{\sum_{k=1} V_{k,p}}{V} \quad (8)$$

where $V_{k,p}$ is the volume of certain particle k and V is the volume of the current mesh cells.

Boundary Conditions

Parabolic Inlet Velocity

There are different breathing patterns for the different levels of activity such as rest, light activity, and moderate exercise (Fenn and Rahn, 1965). The flow velocity distribution at the inlet of an airway is close to a sinusoidal wave and consists of both inhalation and exhalation (Zhang *et al.*, 2002), but the actual cyclic waveform under normal breathing slightly departs from an equivalent sine-waveform. To simplify the approach, the average flow velocity at the inlet is commonly calculated based on a sine waveform. The unsteady inhalation waveforms of an average air flow at the inlet during rest, light activity, and moderate exercise are illustrated in Fig. 2 with the respective waveforms of a real inhalation (Fenn and Rahn, 1965; Zhang *et al.*, 2002). Different levels of activity and their corresponding parameters for the breathing conditions are summarized in Table 2. The average inlet velocity was described at the entrance of the parent branch as shown (Piglione *et al.*, 2012):

$$V_G = \frac{Q_{in} / 2^G}{\pi D_G^{\,2} / 4} \quad (9)$$

where G is the Weibel's lung generation, D is the diameter of branch entrance, and Q_{in} is the flow rate at the inlet. A

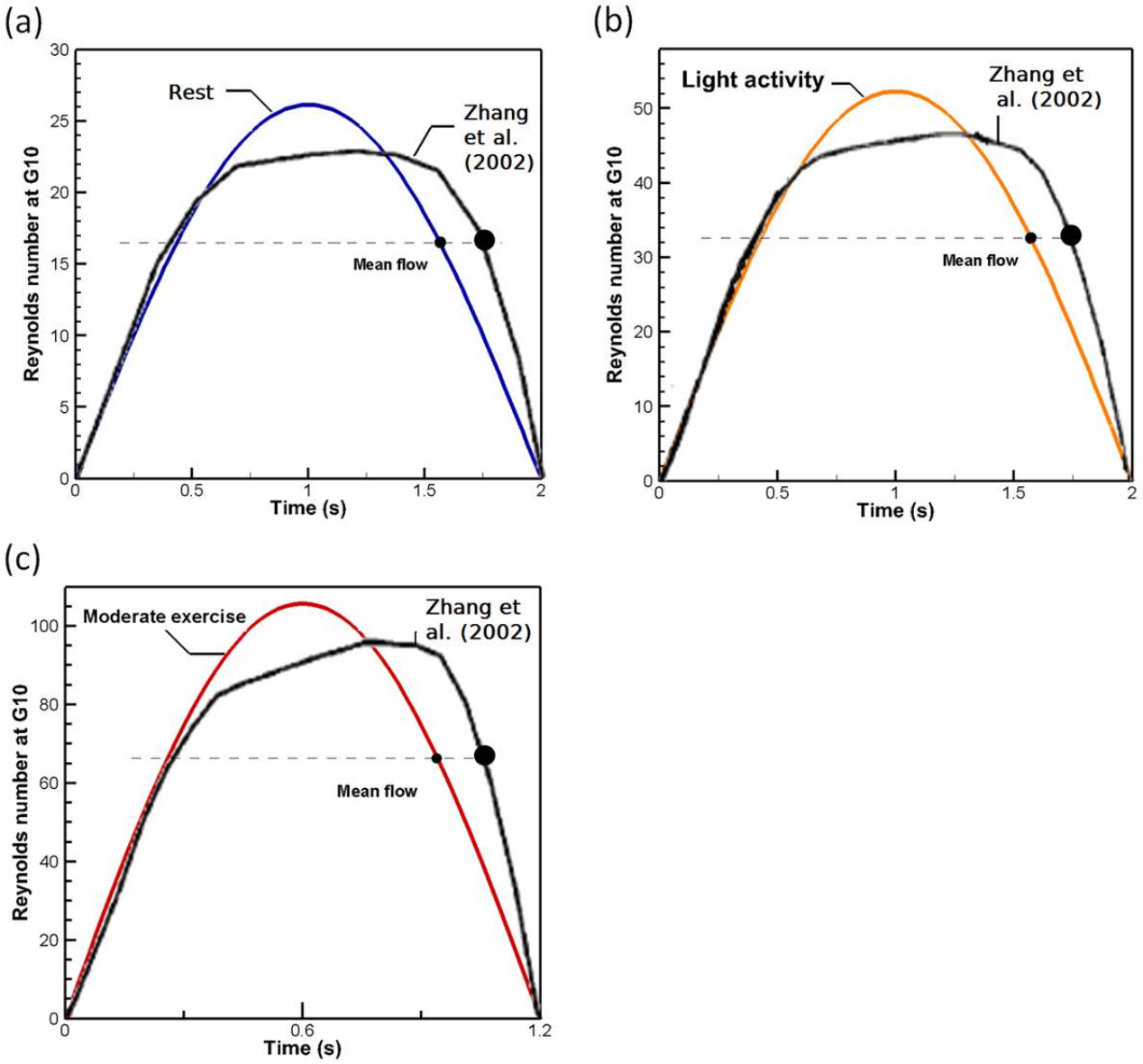

Fig. 2. Schematics of a sinusoidal waveform flow input for the three breathing conditions compared to results from Zhang *et al.* (2002) at (a) rest (15 L min^{-1}), (b) light activity (30 L min^{-1}), and (c) moderate exercise (60 L min^{-1}).

Table 2. Representative inspiratory data.

	Rest	Light activity	Moderate exercise
Respiration rate for inhalation (Q_{in}, L min^{-1})	15.0	30.0	60.0
Time of inhalation cycle (s)	2.0	2.0	1.2
Mean Reynolds number at G10*	16.4	32.7	65.5
Peak Reynolds number at G10	26.6	53.1	108.8

* Generation 10.

fully-developed parabolic velocity profile was employed at the inlet which was created via a user-defined function (UDF) in ANSYS.

Particle Injection and Particle Deposition

The average size distribution of $PM_{2.5}$ suspended in the ambient air of Taiwan with the corresponding percentage concentration is shown in Table 3 (Chen *et al.*, 1997). The density of spherical particles was assumed to be 1.5 g cm^{-3} (Kannosto *et al.*, 2008; Liu *et al.*, 2015). A deterministic-parabolic particle distribution at the inlet of G10 was represented by (Zhang *et al.*, 2001):

$$\frac{C(r)}{C} = 2\left[1-\left(\frac{r}{R}\right)^2\right] \tag{10}$$

Table 3. Average concentrations of $PM_{2.5}$ particle sizes in Taiwan (Chen *et al.*, 1997).

Midpoint diameter (range, μm)	Percentage of $PM_{2.5}$ mass concentration (%)
0.075 (0.05–0.1)	12.32
0.15 (0.1–0.2)	24.72
0.3 (0.2–0.4)	10.46
0.6 (0.4–0.8)	20.04
1.2 (0.8–1.6)	16.55
2.05 (1.6–2.5)	15.91

Note: The mass concentration (%) is the percentage of the measured concentration of $PM_{2.5}$.

where $C(r)$ and C are the local and average particle concentrations, respectively. In a given ring of $r_a \le r \le r_b$, the number of particles (np) is given by (Zhang *et al.*, 2001).

$$n_p = \mathrm{Int}\left[2C\pi\left(r_b^2 - r_a^2 - \frac{r_b^4 - r_a^4}{2R}\right)\right] \quad (11)$$

where R is the radius at the inlet, subscripts a and b are the radii of the preceding and subsequent rings at the inlet, and Int[] is a function that truncated the mathematical statement into an integer.

Particles were released from the entrance into the tube at G10 (Figs. 1(a) and 1(b)) and expelled out of the airways at G11 during inhalation. The particle concentration at the inlet was the same for every time step. The initial inlet particle velocity was also proportional to the inlet axial velocity profiles for each released time step, and the motion of particle at all outlets was set to the "escape" condition. The particle-wall interaction boundary condition was assumed to trap all the particles with a 100% efficiency. This was due to the presence of a mucus lining along the inner wall of lung airways. Uniform (zero) gage pressure was applied at the outlets (Feng and Kleinstreuer, 2014).

Physical Quantities

The Reynolds number of air at the inlet (Re_d) is defined as (Zhang *et al.*, 2002)

$$Re_d = \frac{\rho U_{mean} D}{\mu} \quad (12)$$

where ρ is the air density (= 1.225 kg m^{-3}), μ is the dynamic viscosity (=1.789 × 10^{-5} kg m^{-1} s^{-1}), and D is the airway diameter at G10 whose value is 1.3 × 10^{-3} m (Weibel, 1963b). The flow velocity at the entrance of G0 (i.e., the mouth's entrance) is uniform. But as the flow proceeds from G0 into other generations in the airways, the velocity profile becomes parabolic distribution due to the drag force and no-slip boundary condition developed on walls of the airways. Consequently, the velocity distribution at the inlet of G10 is parabolic where the maximum flow velocity (U_{max}) at the center of the airway's cross-section is equivalent to twice of the average flow velocity (U_{mean}). This assumption was practical and most appropriate for making comparisons (Zhang *et al.*, 2001).

Deposition fraction (DF), a measure of the number percentage of particles getting trapped on the walls (Huang and Zhang, 2011), is defined as

$$DF(\%) = \frac{\text{The number of particles deposited on the walls}}{\text{The number of particles entering that section of the wall}} \times 100 \quad (13)$$

Numerical Method

The geometry of the bifurcations was developed using a graphic software SOLIDWORKS. The mesh was generated based on the non-tetrahedral grids obtained from a commercial software ANSYS 16.0. The numerical solutions of the gas-solid two-phase flow equations were carried out using the finite-volume based program in ANSYS where the SIMPLEC algorithm was adopted in the simulation of multi-phase flow in the respiratory tract bifurcation. SIMPLEC was adopted because the flow during this simulation was assumed to be laminar and the convergence was determined by the pressure-velocity coupling. The momentum equations of the fluid were discretized by a Three-Order MUSCL scheme, while the gradient selection was Green-Gauss Node Based. The standard pressure interpolation scheme was also used. The relaxation velocity coefficient and pressure were set as 0.75. One cycle of respiration was calculated before releasing particles in order to avoid start-up effects on the air-particle flow fields.

The discrete phase model (DPM) which is an Euler-Lagrange hybrid approach, was applied to define the flow of particulate matters. The momentum equations of the continuum were incorporated into the discrete phase particle trajectories. Therefore, the continuous gaseous phase influenced the flow of discrete particulate phase. This two-way coupling solved the discrete and continuous phase equations interchangeably, until the solutions in both phases stopped changing. During the simulation, rest and light activity had 50 time steps each, while moderate activity had 30 time steps to ensure the smoothness of the positive half sinusoidal inhalation cycle. A fixed time step (Δt = 0.04 s) was adopted to calculate the flow fields and particle trajectories. The calculation at each time step was iterated until convergence was achieved where the mass residue in the continuity equation should be less than 10^{-5}.

Model Validation

The results of Zhang *et al.* (2002) were used for numerical validation of the developed method. A grid system with

tetrahedral meshes was built, as shown in Fig. 1(c), where the total number of the mesh elements was 1,383,095 with 252,915 nodes. The computational domain covered generations 3–6 (G3–G6), and the average inlet Reynolds number was 805. At the initial stage of the first inhalation flow, 18,000 particles were released into the airways, and a parabolic distribution of particles at the inlet was used (Zhang *et al.*, 2001). Fig. 3(a) shows the velocity vectors and contours between G3 and G6 where the breathing time was 1.0 s. Figs. 3(b)–3(d) display the velocity vectors and contours at different cross-sectional areas at 1.0 s. It can be seen that vortices formed in G4 and G5 airways. The axial velocity distributions in Fig. 3(b) show that the high flow rate is skewed towards side B. Fig. 3(c) shows the change in axial velocity which has an eccentric distribution and velocity vector in the cross-section C-C'. The velocities in Fig. 3(c) are lower compared to those in Fig. 3(d). The cross section D-D' in Fig. 3(d) has two vortices and they are more intense compared to those in the cross-section C-C'. Fig. 3(e) shows the particle deposition patterns under one cycle inhalation. Overall, the phenomena obtained in the present work are in line with the results of Zhang *et al.* (2002), thereby validating the developed model.

Grid Independence

Prior to simulations the mesh independence of the computational domain was ensured by comparing the results from three different meshes of 756,424 (Mesh 1), 1,171,561 (Mesh 2), and 1,483,376 (Mesh 3) elements. The study focused on a transient inhalation under light activity where the average air Reynolds number and average hourly concentration of $PM_{2.5}$ at the inlet were 32.7 and 117 μg m^{-3}, respectively. Meanwhile, 42,336 particles with a particle diameter of 0.075 μm, 10,608 particles with a diameter of 0.15 μm, 576 with a diameter of 0.3 μm, and 144 with a diameter of 0.6 μm were injected under the light activity inhalation condition. The profiles of DF of particles at the four different particle sizes are shown in Fig. 4. The values of DF based on Mesh 2 are close to those based on Mesh 3 where the maximum relative error was around 6.6 % as shown in Table 4. This implies, in turn, that 1,171,561 tetrahedral elements were sufficient to predict DF and thus adopted for the two-phase flow simulations in this study.

RESULTS AND DISCUSSION

Air Flows in Healthy Airways

The variation of air flow velocity with time for a single inhalation at the inlet is assumed to conform to a positive half cycle of a sine wave. Three different breathing conditions are used for this study; they are rest, light activity, and moderate exercise, as shown in Fig. 2. To determine the number of $PM_{2.5}$ particles inhaled during the three activities, the total number of particles are equally distributed among the time steps to obtain the average number of particles injected during a single time step of 0.04 s, as indicated in Table 5. The concentration of $PM_{2.5}$ in the ambient air employed for the simulations is 1.5 g cm^{-3} (Kannosto *et al.*, 2008). According to the distribution of particles at the inlet shown in Fig. 5, the highest number of particles for all diameters are inhaled during moderate exercise, while the least are inhaled during the rest condition. For each inhalation cycle, the initial velocity of the particles at the inlet is set to be equal to the air flow velocity (the entrance of G10) (Zhang *et al.*, 1997).

Peak flows are usually applied in numerical simulations for airflow in the human airways to represent the transient flow (Piglione *et al.*, 2012). Therefore, the maximum air flow velocity occurring at the inhalation time of 1.0 s (Fig. 2) is used to show the flow velocity variations for inhalation during rest, light activity, and moderate exercise (Piglione *et al.*, 2012). The axial velocity contours and streamlines distribution for a healthy bifurcation under the three inhalation statuses are shown in Figs. 6(a)–6(c). The cross-sectional areas for G10 and G11 are 16.4 and 23.28 mm^2, respectively. On account of the larger area of G11 than G10, the axial velocity in G11 is smaller than that in G10, regardless of the inhalation status. When air flows from G10 to G11, a flow bifurcation occurs, rendering the inclination of streamlines. The maximum Reynolds number is 108.8 (Table 2) for moderate exercise (Fig. 2(c)) which pertains to a laminar flow. Consequently, the streamlines are smooth and no flow separation is exhibited in the airways.

In order to figure out the flow dynamics in the vicinity of the entrances of G11, the velocity vectors and axial velocity contours at the cross-section B-B' are shown in Fig. 7. It is evident that the contour cores are closer to side B. This is attributed to the centrifugally induced pressure gradient which pushes the flow bias toward the inner wall (side B) (Zhang *et al.*, 2002). This centrifugal force further drives the formation of two vertically symmetrical recirculation flows termed the Dean vortices (Dean, 1927). For the case of rest, the Dean vortices are not pronounced (Fig. 7(a)), whereas they become significant at light activity and moderate exercise (Figs. 7(b) and 7(c)). These results clearly reveal that the generation and intensity of the Dean vortices strongly depend on the Reynolds number or flow velocity (Kim and Lee, 2009). The enhanced Dean vortices are responsible for the higher axial velocity contours located at the places adjacent to the carina region of the branched airways in G11 (Figs. 6(b) and 6(c)).

Particle Deposition in Healthy Airways

The profiles of mass deposition fraction and undeposited mass of the inhaled particles are shown in Fig. 8. For the conditions of rest and light activity, DF is zero, implying that no particles are deposited during the inhalation. This presumably arises from the fact that the small particles do not deviate from the streamlines of the flow (Fig. 6), stemming from low Reynolds numbers and thereby inertial force. Therefore, the particles that remain airborne are easily expelled through the pressure outlet of the airways for rest and light activity (Kim and Iglesias, 1989; Nazridoust and Asgharian, 2008). However, the studies of Piglione *et al.* (2012) and Feng *et al.* (2016) found out that for inhalation during rest, a high concentration of fine particulates advanced to the alveolar region where they might cause harm (Piglione *et al.*, 2012; Feng *et al.*, 2016).

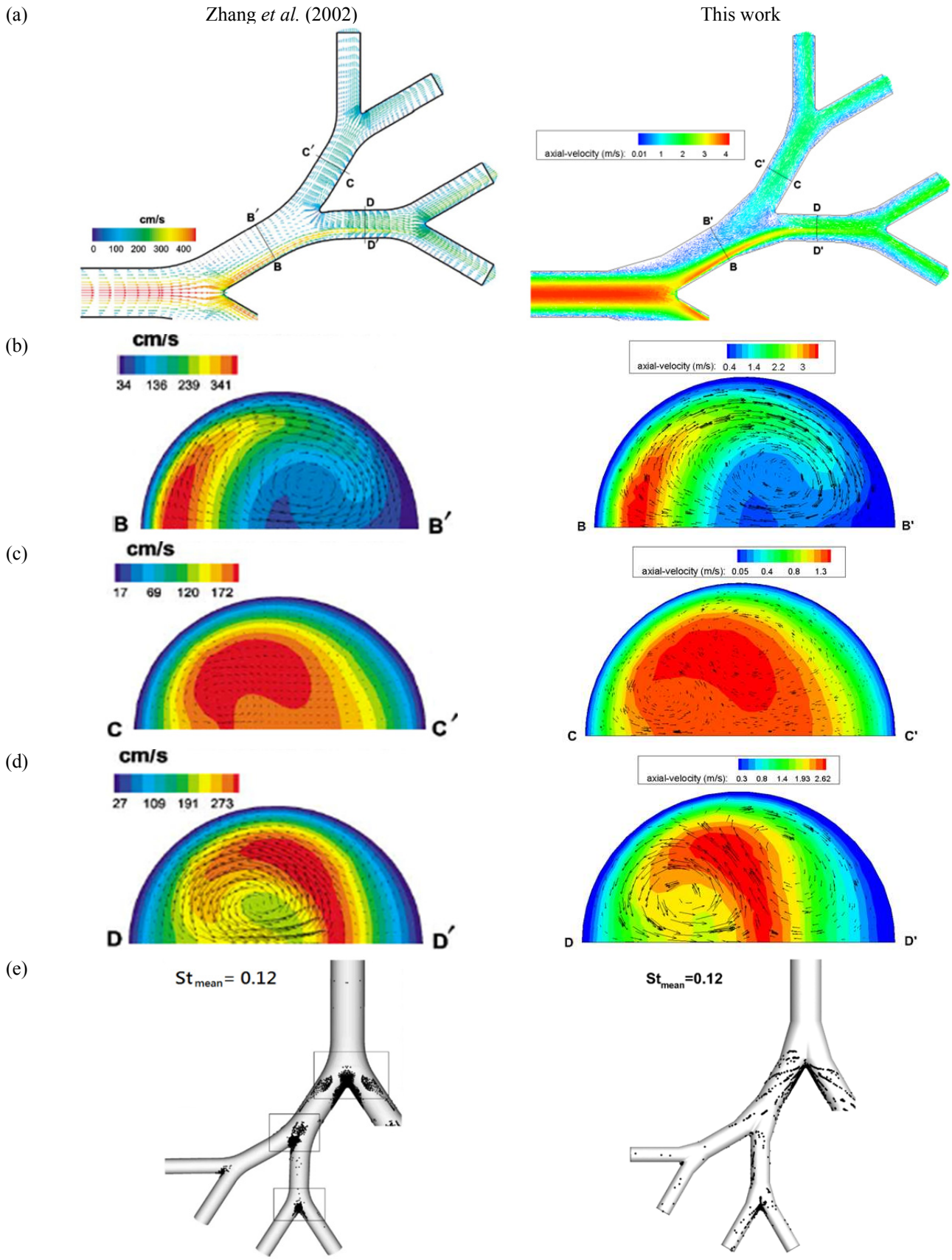

Fig. 3. Mid-plane velocity vectors, and axial velocity contours, secondary velocity vectors at selected cross-sections at 1.0 s of transient inlet condition: (a) G3 to G6; (b) section B-B'; (c) section C-C'; (d) section D-D'; and (e) 3D views of local particle deposition patterns under cyclic inhalation for light activity condition.

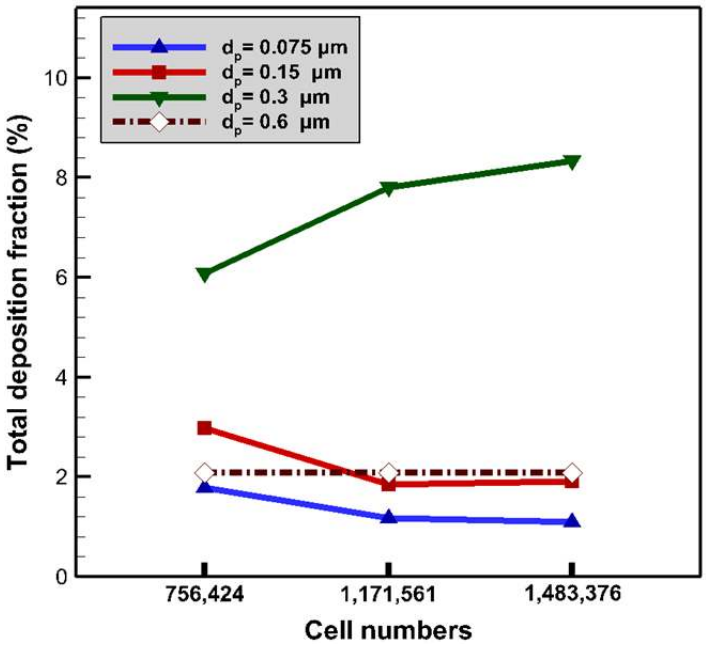

Fig. 4. Grid independent test of two-generations where G10 is healthy while the two G11 are asthmatic.

Table 4. Deposition fraction (%) in asthmatic airways under three different grid systems.

Particle size (μm)	Grid system			Error*
	1	2	3	(1) → (3)
0.075	1.79	1.17	1.10	52.9% → 5.9%
0.15	2.98	1.85	1.91	61.0% → 3.2%
0.3	6.08	7.81	8.33	22.2% → 6.6%
0.6	2.08	2.08	2.08	0.0% → 0.0%
Number of meshes	756,424	1,171,561	1,483,376	

*: Relative error value based on Mesh 2.

Table 5. Total number of particles inhaled during one inspiratory cycle.

Particle size	P_{d1}	P_{d2}	P_{d3}	P_{d4}
Rest	9,120[a]	2,304[a]	N/A[b]	N/A[b]
Light activity	18,192[a]	4,560[a]	240[a]	N/A[b]
Moderate exercise	21,812[a]	5,488[a]	308[a]	84[a]

[a] Particle diameter P_{d1} = 0.075 μm, P_{d2} = 0.15 μm, P_{d3} = 0.3 μm, P_{d4} = 0.6 μm.
[b] no particle input.

For the case of moderate exercise, particle deposition develops where the value of DF is 0.031%. The deposition of the particles in G10 and G11 during moderate exercise is demonstrated in Fig. 9. The particle deposition takes place at three locations, with one (P1) in G10 and the other two (P2 and P3) in G11. Physically, the Reynolds number is the ratio of inertial force to viscous force within a fluid. The Reynolds number for moderate exercise is higher, suggesting that air in the airways has a higher inertial force compared to the air during rest and light activity. This results in the deposition of particles at P1 where the dominant mechanism is inertial impaction around the bifurcation point (Nazridoust and Asgharian, 2008; Piglione *et al.*, 2012). In contrast, for the deposition at P2 and P3, it is inferred that the mechanism is governed by the intensified secondary flows or Dean vortices, giving rise to the impaction of particles onto the walls (Fig. 7(c)). Overall, the predicted deposition phenomena under the rest and moderate exercise are in line with the results of Daigle *et al.* (2003)

Air Flows in Asthmatic Airways

The airway geometry of G10 and G11 is shown in Fig. 1(b). The number of grids selected is 1,171,561 elements (Fig. 4). Both the healthy airway (G10) and asthmatic airways (G11) were constructed using tetrahedral grids (Fig. 1(d)). However, the meshes were more refined for G11 which was affected by bronchus asthma due to the need to accurately capture the deposition and flow fields (Huang and Zhang, 2011; Piglione *et al.*, 2012). The mid-plane axial velocity contours and vectors during inhalation for

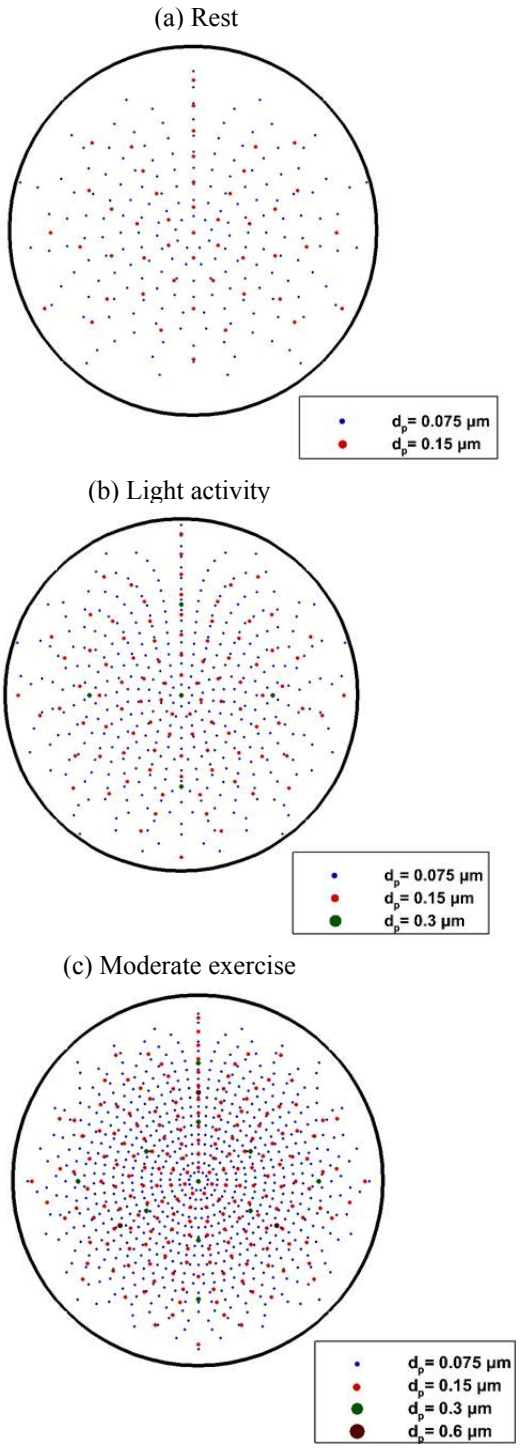

Fig. 5. Particle inlet positions with distribution deterministic-parabolic (Zhang and Kleinstreuer, 2001) for (a) Rest, (b) light activity, and (c) Moderate exercise condition.

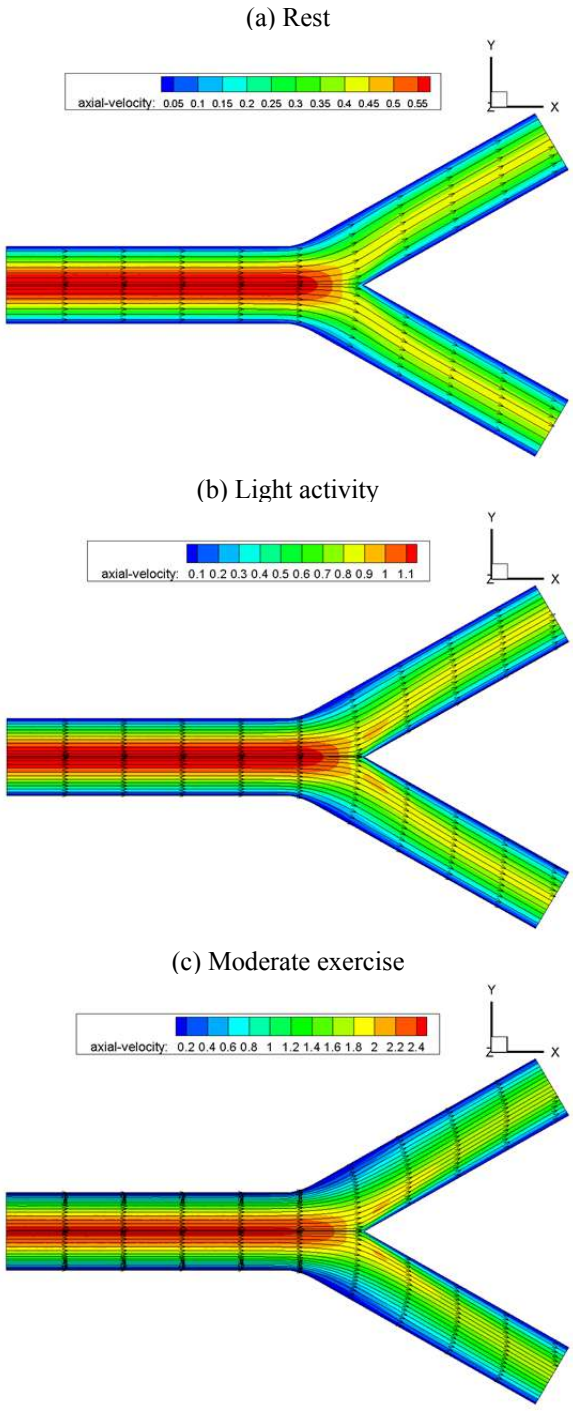

Fig. 6. Mid-plane streamline and axial velocity contours at the peak flow during the inspiratory phase where G10 and G11 are healthy (a) rest, (b) light activity, and (c) Moderate exercise condition.

the three breathing conditions are presented in Fig. 10. The vectors change substantially before and after the transition between G10 and G11 due to the size of the folds. The areas of G10 (healthy) and G11 (asthmatic) in Fig. 10 are 16.4 and 9.31 mm^2, respectively. In view of the sudden contraction in the area at the location between G10 and G11, there is an accelerated flow in the asthmatic generation (G11) and the axial velocity is markedly amplified, irrespective of the breathing situation. As a result, the parabolic velocity profiles in G11 become sharper, especially for the moderate exercise (Fig. 10(c)).

The differences in axial velocity contours and velocity vectors at cross-sections A-A' and B-B' in the asthmatic airway are shown in Fig. 11. For A-A', the axial velocity is

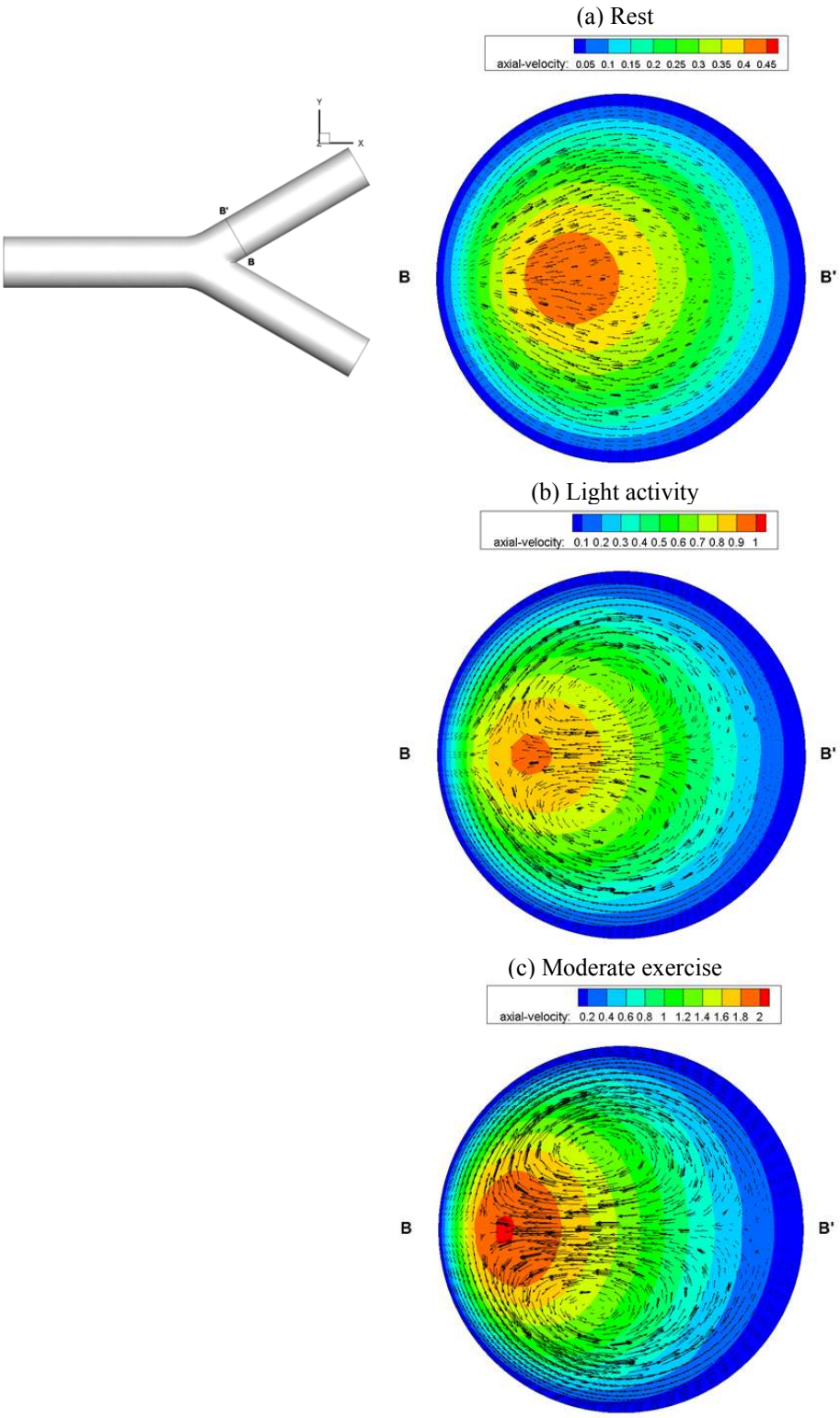

Fig. 7. Section B-B' velocity vectors, and axial velocity contours at the time level of peak flow rate during inhalation where G10 and G11 are healthy at (a) rest, (b) light activity, and (c) moderate exercise condition.

also pushed towards side A, and a pair of vertically symmetrical secondary flows (Dean vortices) due to the centrifugal force are observed. For the low flow rate at rest, the secondary flow phenomenon is less distinct, and the velocity contour core is slightly skewed towards side A (Fig. 11(a)). As regards to moderate exercise, the higher Reynolds number intensifies the centrifugal force so the core approaches the inner wall more (Fig. 11(c)). In section B-B' (Fig.11), it is observed that after the contraction of the tube, the reduced radius and geometric shape of the

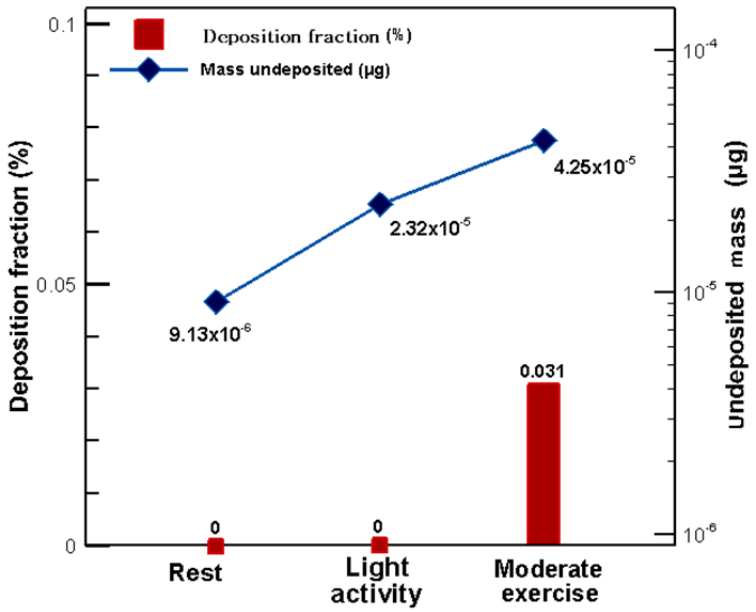

Fig. 8. Total mass deposition fraction and mass that remains suspended in the two-generation healthy airway.

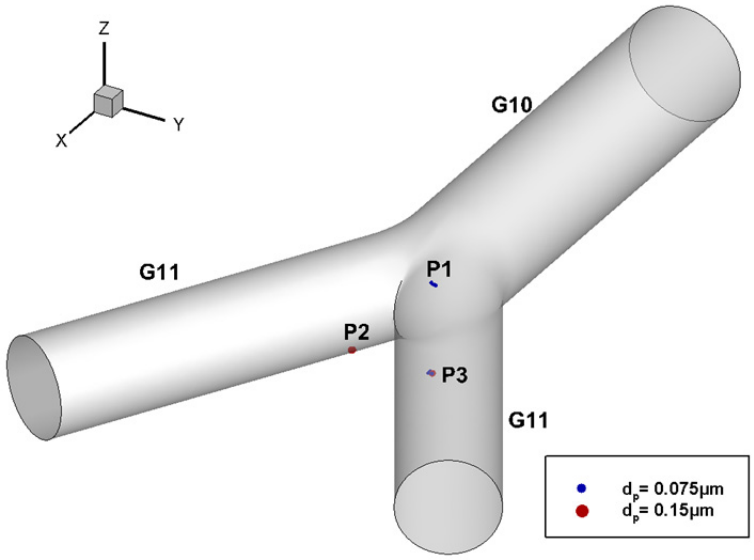

Fig. 9. Deposition of $PM_{2.5}$ during moderate exercise in the two-generation healthy airway.

tube corrugation lead to increased fluid velocity and complex secondary flow patterns (Zhang *et al.*, 2001). Air flows at section B-B' are not affected by the centrifugal forces because they are far from the bifurcation. As a consequence, the axial velocity contour cores at B-B' are located at the center of the asthmatic airway.

Particle Deposition in the Asthmatic Airway

Particle deposition patterns during inhalation for the three breathing types at the $PM_{2.5}$ concentration of 50 μg m^{-3} injected into the airways are displayed in Fig. 12. There is no deposition in G10 whether the breathing is during rest, light activity, or moderate exercise. The particles follow the air motion, with deposition first occurring at the place before the carina region. This is mainly attributed to the inertial forces of the particles (Choi *et al.*, 2007). The induced Dean vortices facilitate the chances of the particles touching the wall surfaces. Consequently, more particles get deposited in the asthmatic airways. The higher the Reynolds number or air flow rate, the more drastic the particle deposition phenomena. A comparison to G11 of the healthy airway (Fig. 9) suggests that particle deposition in G11 of the asthmatic airways (Fig. 12(c)) is more obvious. This verifies the fact that, deformed airways make it easy for the $PM_{2.5}$ to be captured, thereby deteriorating the breathing situation.

The profiles of DF of particles with different sizes and mass deposited in G10 and G11of the asthmatic airways during inhalation under the three breathing conditions are shown in Fig. 13. It appears that an increase in particle

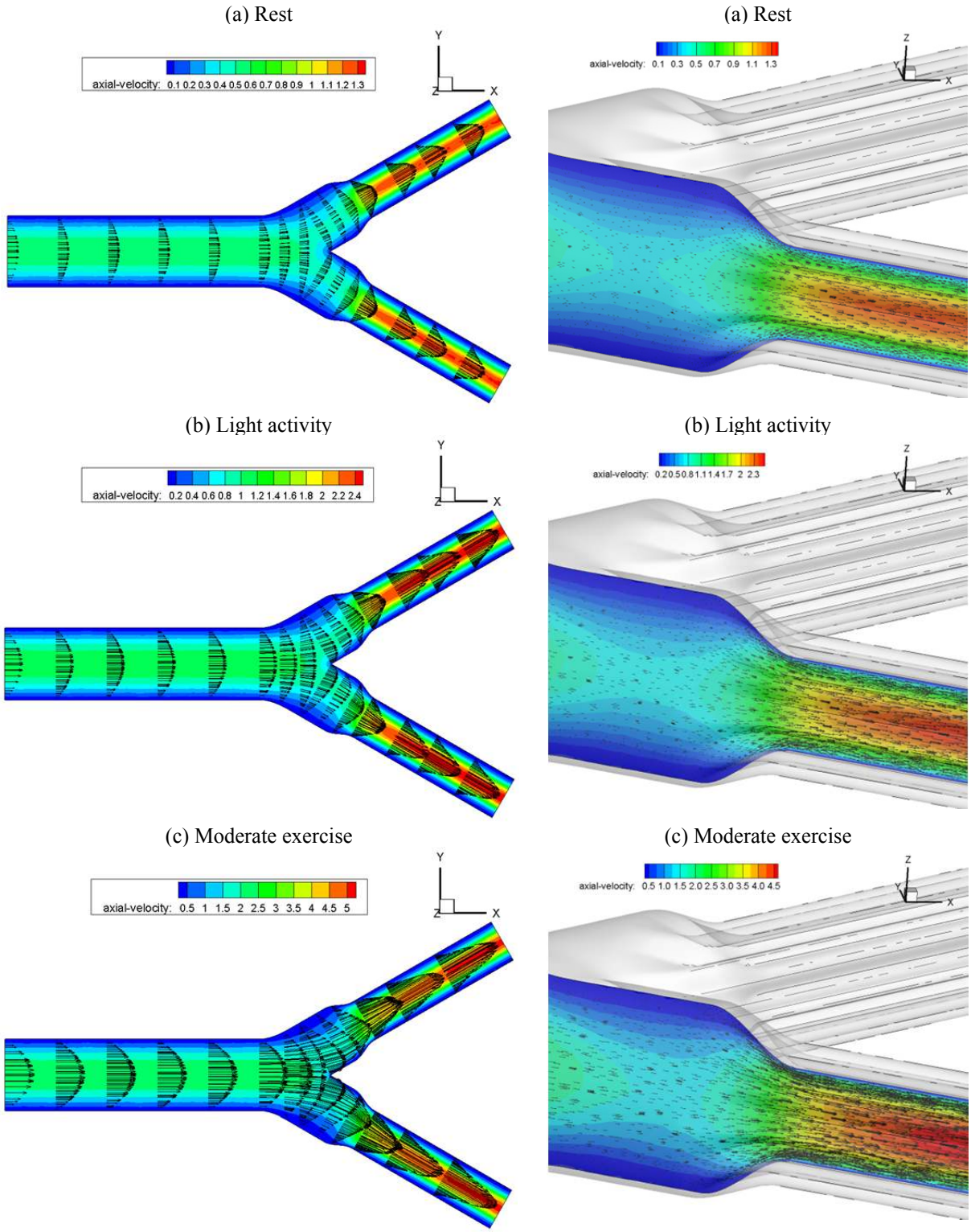

Fig. 10. Mid-plane velocity vectors, axial velocity contours, tapering velocity vectors, and axial velocity contours at the time level of peak flow rate during the inspiratory phase where G10 is healthy while the two G11 are asthmatic for (a) rest, (b) light activity, and (c) moderate exercise condition.

diameter substantially increases DF. For example, for moderate exercise, the values of DF corresponding to the particle sizes of 0.075, 0.15, 0.3, and 0.6 μm are 1.19, 2.53, 14.3 and 25.0%, respectively. Total particle deposition was highest during moderate activity. Light activity also had a higher particle deposition compared to deposition during rest. The particle deposition mass during rest was 8.32×10^{-8} μg, and increased to 6.31×10^{-7} μg and 4.95×10^{-8} μg

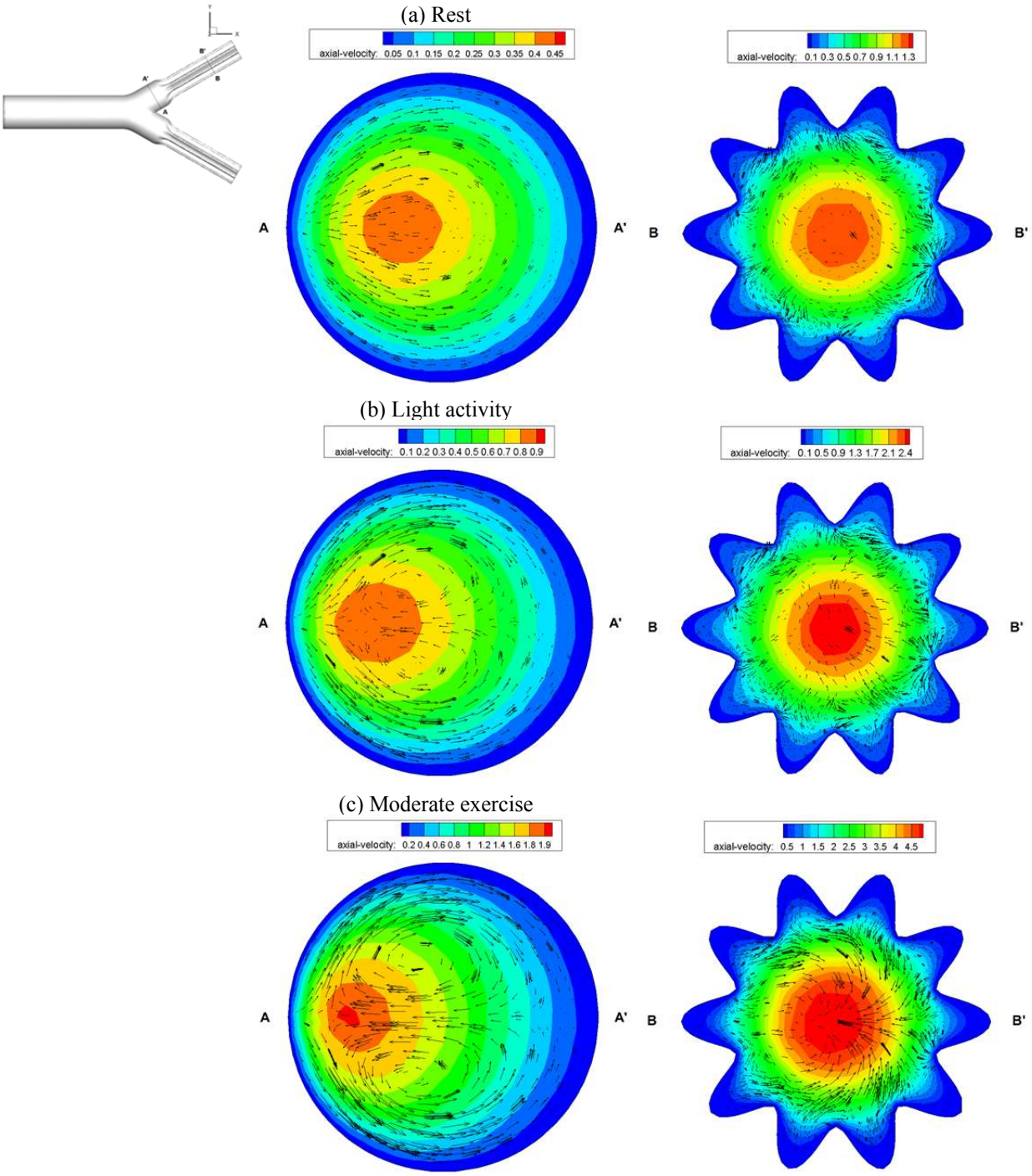

Fig. 11. A and B section velocity vectors, and axial velocity contours at the time level of peak flow rate during the inspiratory phase where G10 is healthy while the two G11 are asthmatic for (a) Rest, (b) Light activity, and (c) Moderate exercise condition.

under light activity and moderate exercise, respectively. Overall, this trend matched with the results from a study by Chalupa *et al.* (2004).

Comparison of Healthy Airways and Asthmatic Airways

Fig. 8 has shown that $PM_{2.5}$ deposition in G10 and G11 for the healthy human airways was zero, and therefore the fine particles still remained suspended within the human respiratory tract, and possibly ended up reaching the alveolar region. A study by Piglione *et al.* (2012) indicated that Reynolds number was very small at the lower generations of human airways, while a parabolic velocity distribution developed in a cross-sectional area showed that the inertial forces at the lower generations were insignificant. Consequently, deposition rates at these generations were very low because the particles were extremely fine and light,

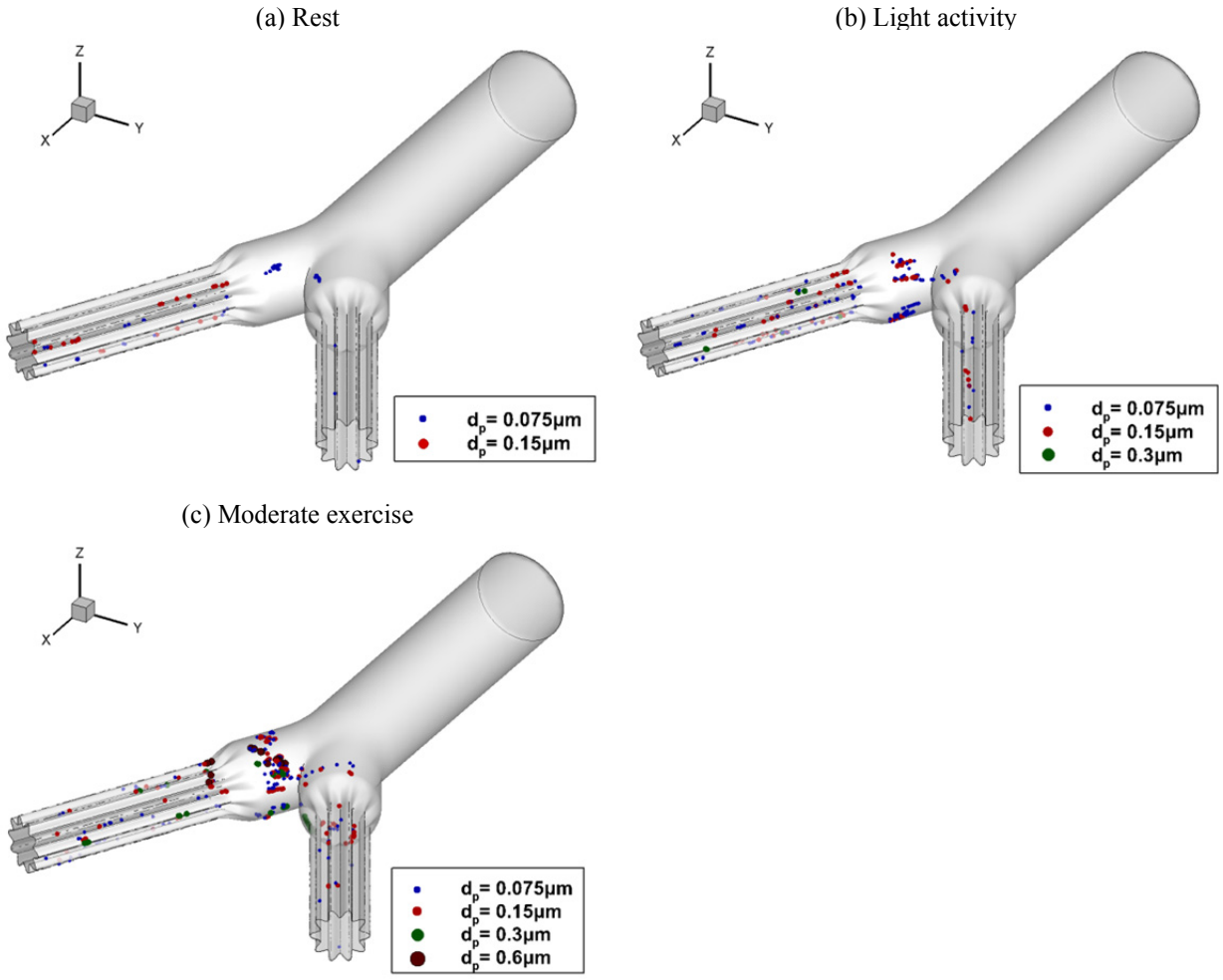

Fig. 12. Deposition of $PM_{2.5}$ where G10 is healthy while the two G11 are asthmatic for (a) rest, (b) light activity, and (c) moderate exercise condition in the two-generation asthmatic airways.

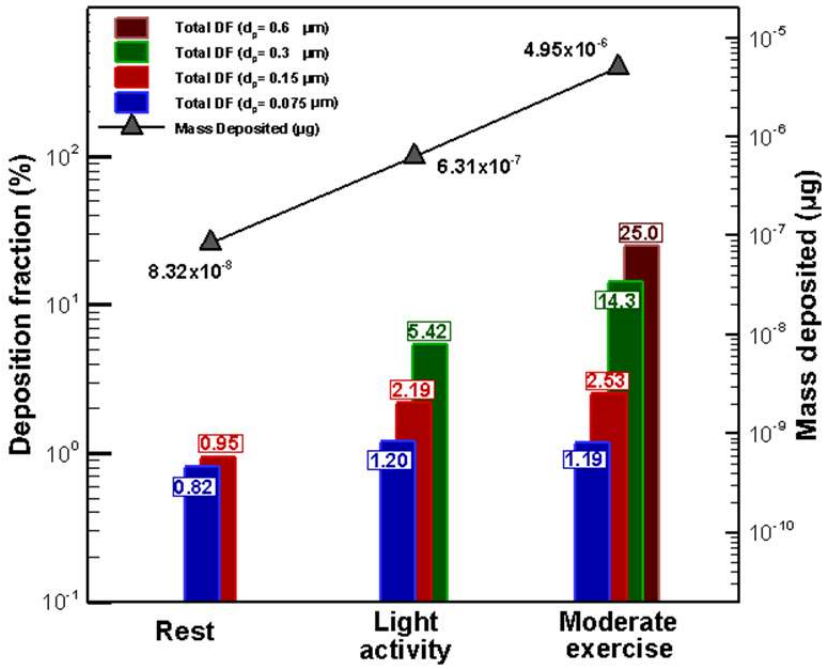

Fig. 13. Deposition fraction and mass deposited where G10 is healthy while the two G11 are asthmatic.

and thus their inertial forces were very low and incapable of causing deposition (Choi *et al.*, 2007). Consequently, the particles that remained airborne at the end of the inhalation cycle could either be expelled to the surrounding or get deposited in the upper bronchial airways during exhalation (Inthavong *et al.*, 2010).

A comparison between Fig. 8 and Fig. 13 has depicted that the asthmatic human airways had a higher c deposition compared to a healthy human airways. This characteristic was also demonstrated by a previous study whereby exposure of asthmatic human airways to $PM_{2.5}$ decreased clearance of bacteria resulting in impaired defense of the affected generation (Vempilly *et al.*, 2013) Therefore, for the same concentration of fine particulate matter suspended in the ambient air, the concentration of particulate matter deposited in the airways of an asthmatic patient is higher than deposition for a healthy individual. This further increases the risk of adverse health effects for asthmatic individuals (McCreanor *et al.*, 2007).

CONCLUSIONS

The flow fields and $PM_{2.5}$ deposition in generation 10 and 11 (G10 and 11) of healthy and asthmatic airways under three different breathing conditions, namely, rest, light activity, and moderate exercise, have been investigated using computational fluid dynamics. For the flow fields, Dean vortices developed in the area adjacent to the entrance of G11 and were closer to the inner walls, for both healthy or asthmatic airways. The secondary flows exhibited was attributed to induced centrifugal forces. For the healthy airways, no particle deposition was observed under rest and light activity, whereas the deposition fraction (DF) was 0.031% at moderate exercise condition where the deposition mechanisms were contributed by inertial impaction and Dean vortices before and after the bifurcation, respectively. The deposition fraction in an asthmatic human airways was higher than that of a normal human airway. The Dean vortices induced by the deformed airways increased the likelihood of particles touching the walls of the airways, thereby increasing the transient deposition fraction of $PM_{2.5}$ in the asthmatic airway walls. $PM_{2.5}$ deposition was also greatly influenced by the size of the particulate matters, and increased with an increase in the diameter of fine particulates. Dean vortices in the asthmatic airways were not pronounced during rest, but they became significant during light activity and moderate exercise. These findings have significance implications on the effects of activity level on $PM_{2.5}$ deposition for asthmatic patients.

ACKNOWLEDGMENTS

The authors gratefully acknowledge the financial support (MOST 106-2923-E-006-002-MY3) of the Ministry of Science and Technology, Taiwan, ROC, for this study.

REFERENCES

Chalupa, D.C., Morrow, P.E., Oberdörster, G., Utell, M.J. and Frampton, M.W. (2004). Ultrafine particle deposition in subjects with asthma. *Environ. Health Perspect.* 112: 879.

Chen, S.J., Liao, S.H., Jian, W.J. and Lin, C.C. (1997). Particle size distribution of aerosol carbons in ambient air. *Environ. Int.* 23: 475–488.

Chen, W.H. (2001a). Dynamics of sulfur dioxide absorption in a raindrop falling at terminal velocity. *Atmos. Environ.* 35: 4777–4790.

Chen, W.H. (2001b). Unsteady absorption of sulfur dioxide by an atmospheric water droplet with internal circulation. *Atmos. Environ.* 35: 2375–2393.

Chen, W.H., Chen, Y.Y. and Hung, C.I. (2011). A simplified model of predicting SO_2 absorption by single atmospheric raindrops with chemical dissociation and internal circulation. *Aerosol Air Qual. Res.* 11: 860–872.

Chen, W.H., Tsai, M.H. and Hung, C.I. (2014). Characterization of transient CO_2 transport in two convecting aerosol droplets in tandem. *Aerosol Air Qual. Res.* 14: 207–219.

Choi, L.T., Tu, J., Li, H. and Thien, F. (2007). Flow and particle deposition patterns in a realistic human double bifurcation airway model. *Inhalation Toxicol.* 19: 117–131.

Daigle, C.C., Chalupa, D.C., Gibb, F.R., Morrow, P.E., Oberdörster, G., Utell, M.J. and Frampton, M.W. (2003). Ultrafine particle deposition in humans during rest and exercise. *Inhalation Toxicol.* 15: 539–552.

Dean, W. (1927). XVI. Note on the motion of fluid in a curved pipe. *London,. Edinburgh, Dublin Philos. Mag. J. Sci.* 4: 208–223.

Donaldson, K., Stone, V., Clouter, A., Renwick, L. and MacNee, W. (2001). Ultrafine particles. *Occup. Environ. Med.* 58: 211–216.

Donovan, G.M. and Tawhai, M.H. (2010). A simplified model of airway narrowing due to bronchial mucosal folding. *Respir. Physiol. Neurobiol.* 171: 144–150.

Ebina, M., Yaegashi, H., Chiba, R., Takahashi, T., Motomiya, M. and Tanemura, M. (1990). Hyperreactive site in the airway tree of asthmatic patients revealed by thickening of bronchial muscles: A morphometric study. *Am. Rev. Respir. Dis.* 141: 1327–1332.

Feng, J., Yu, H., Liu, S., Su, X., Li, Y., Pan, Y. and Sun, J. (2016). $PM_{2.5}$ levels, chemical composition and health risk assessment in Xinxiang, a seriously air-polluted city in North China. *Environ. Geochem. Health* 39: 1071–1083.

Feng, Y. and Kleinstreuer, C. (2014). Micron-particle transport, interactions and deposition in triple lung-airway bifurcations using a novel modeling approach. *J. Aerosol Sci.* 71: 1–15.

Fenn, W.O. and Rahn, H. (1965). Handbook of physiology: Section 3. *Anesthesiology* 26: 366–366.

He, K., Yang, F., Ma, Y., Zhang, Q., Yao, X., Chan, C.K., Cadle, S., Chan, T. and Mulawa, P. (2001). The characteristics of $PM_{2.5}$ in Beijing, China. *Atmos. Environ.* 35: 4959–4970.

Hofmann, W., Balásházy, I. and Koblinger, L. (1995). The The effect of gravity on particle deposition patterns in

bronchial airway bifurcations. *J. Aerosol sci.* 26: 1161–1168.

Horsfield, K., Dart, G., Olson, D.E., Filley, G.F. and Cumming, G. (1971). Models of the human bronchial tree. *J. Appl. Phys.* 31: 207–217.

Hrousis, C.A., Wiggs, B.J., Drazen, J.M., Parks, D.M. and Kamm, R.D. (2002). Mucosal folding in biologic vessels. *J. Biomech. Eng.* 124: 334–341.

Huang, J. and Zhang, L. (2011). Numerical simulation of micro-particle deposition in a realistic human upper respiratory tract model during transient breathing cycle. *Particuology* 9: 424–431.

Inthavong, K., Choi, L.T., Tu, J., Ding, S. and Thien, F. (2010). Micron particle deposition in a tracheobronchial airway model under different breathing conditions. *Med. Eng. Phys.* 32: 1198–1212.

Jain, V.V., Abejie, B., Bashir, M.H., Tyner, T. and Vempilly, J. (2013). Lung volume abnormalities and its correlation to spirometric and demographic variables in adult asthma. *J. Asthma* 50: 600–605.

Johnson, P.C. and Jackson, R. (1987). Frictional-collisional constitutive relations for granular materials, with application to plane shearing. *J. Fluid Mech.* 176: 67–93.

Kannosto, J., Lemmetty, M., Virtanen, A., Mäkelä, J., Keskinen, J., Junninen, H., Hussein, T., Aalto, P. and Kulmala, M. (2008). Mode resolved density of atmospheric aerosol particles. *Atmos. Chem. Phys.* 8: 5327–5337.

Khlystov, A., Stanier, C. and Pandis, S. (2004). An algorithm for combining electrical mobility and aerodynamic size distributions data when measuring ambient aerosol special issue of aerosol science and technology on findings from the fine particulate matter supersites program. *Aerosol Sci. Technol.* 38: 229–238.

Kim, C.S. and Iglesias, A.J. (1989). Deposition of inhaled particles in bifurcating airway models: I. Inspiratory deposition. *J. Aerosol Med.* 2: 1–14.

Kim, S. and Lee, S.J. (2009). Measurement of Dean flow in a curved micro-tube using micro digital holographic particle tracking velocimetry. *Exp. Fluids* 46: 255.

Kuo, Y.M., Hung, H.F. and Yang, T.T. (2007). Chemical compositions of $PM_{2.5}$ in residential homes of southern Taiwan. *Aerosol Air Qual. Res.* 7: 403–416.

Lambert, R., Codd, S., Alley, M. and Pack, R. (1994). Physical determinants of bronchial mucosal folding. *J. Appl. Phycol.* 77: 1206–1216.

Lee, K.L., Lee, W.J., Mwangi, J.K., Wang, L.C., Gao, X. and Chang-Chien, G.P. (2016). Atmospheric $PM_{2.5}$ and depositions of polychlorinated dibenzo-*p*-dioxins and dibenzofurans in Kaohsiung area, southern Taiwan. *Aerosol Air Qual. Res.* 16: 1775–1791.

Lin, C.H., Wu, Y.L., Lai, C.H., Watson, J.G. and Chow, J.C. (2008). Air quality measurements from the southern particulate matter supersite in Taiwan. *Aerosol Air Qual. Res.* 8: 233-264.

Liu, Z., Hu, B., Ji, D., Wang, Y., Wang, M. and Wang, Y. (2015). Diurnal and seasonal variation of the $PM_{2.5}$ apparent particle density in Beijing, China. *Atmos. Environ.* 120: 328–338.

Macklem, P.T. (1996). A theoretical analysis of the effect of airway smooth muscle load on airway narrowing. *Am. J. Respir. Crit. Care Med.* 153: 83–89.

McCreanor, J., Cullinan, P., Nieuwenhuijsen, M.J., Stewart Evans, J., Malliarou, E., Jarup, L., Harrington, R., Svartengren, M., Han, I.K. and Ohman Strickland, P. (2007). Respiratory effects of exposure to diesel traffic in persons with asthma. *N. Engl. J. Med.* 357: 2348–2358.

Morawska, L., Johnson, G., Ristovski, Z. and Agranovski, V. (1999). Relation between particle mass and number for submicrometer airborne particles. *Atmos. Environ.* 33: 1983–1990.

Morel, C. (2015). *Mathematical modeling of disperse two-phase flows.* Springer, New York.

Morsi, S. and Alexander, A. (1972). An investigation of particle trajectories in two-phase flow systems. *J. Fluid Mech.* 55: 193–208.

Nazridoust, K. and Asgharian, B. (2008). Unsteady state airflow and particle deposition in a three-generation human lung geometry. *Inhalation Toxicol.* 20: 595–610.

Piglione, M.C., Fontana, D. and Vanni, M. (2012). Simulation of particle deposition in human central airways. *Eur. J. Mech. B. Fluids* 31: 91–101.

Rees, S.L., Robinson, A.L., Khlystov, A., Stanier, C.O. and Pandis, S.N. (2004). Mass balance closure and the federal reference method for $PM_{2.5}$ in Pittsburgh, Pennsylvania. *Atmos. Environ.* 38: 3305–3318.

Schauer, J.J., Kleeman, M.J., Cass, G.R. and Simoneit, B.R. (2002). Measurement of emissions from air pollution sources. 5. C_1–C_{32} organic compounds from gasoline-powered motor vehicles. *Environ. Sci. Technol.* 36: 1169–1180.

Tang, H., Cui, K., Xing, J., Zhu, J., Lee, W.J., Mwangi, J.K. and Lee, Y.C. (2017). Part I: $PM_{2.5}$ and polychlorinated dibenzo-*p*-dioxins and dibenzofurans (PCDD/Fs) in the ambient air of southern China. *Aerosol Air Qual. Res.* 17: 1550–1569.

Tsai, H.H., Yuan, C.S., Hung, C.H. and Lin, C. (2011). Physicochemical properties of $PM_{2.5}$ and $PM_{2.5-10}$ at inland and offshore sites over southeastern coastal region of Taiwan Strait. *Aerosol Air Qual. Res*. 11: 664–678.

Vempilly, J., Abejie, B., Diep, V., Gushiken, M., Rawat, M. and Tyner, T.R. (2013). The synergetic effect of ambient $PM_{2.5}$ exposure and rhinovirus infection in airway dysfunction in asthma: A pilot observational study from the Central Valley of California. *Exp. Lung Res.* 39: 434–440.

Wang, W., Shao, L., Guo, M., Hou, C., Xing, J. and Wu, F. (2017a). Physicochemical properties of individual airborne particles in Beijing during pollution periods. *Aerosol Air Qual. Res.* 17: 3209–3219.

Wang, Z., Itahashi, S., Uno, I., Pan, X., Osada, K., Yamamoto, S., Nishizawa, T., Tamura, K. and Wang, Z. (2017b). Modeling the long-range transport of particulate matters for january in east Asia using NAQPMS and CMAQ. *Aerosol Air Qual. Res.* 17: 3065–3078.

Weibel, E.R. (1963a). Geometric and dimensional airway

models of conductive, transitory and respiratory zones of the human lung. In *Morphometry of the human lung*, Weibel, E.R. (Ed.), Springer Berlin Heidelberg, Berlin, Heidelberg, pp. 136–142.

Weibel, E.R. (1963b). Geometry and dimensions of airways of conductive and transitory zones. In *Morphometry of the human lung*, Weibel, E.R. (Ed.), Springer Berlin Heidelberg, Berlin, Heidelberg, pp. 110–135.

Wiggs, B.R., Hrousis, C.A., Drazen, J.M. and Kamm, R.D. (1997). On the mechanism of mucosal folding in normal and asthmatic airways. *J. Appl. Phycol.* 83: 1814–1821.

Xing, J., Cui, K., Tang, H., Lee, W.J., Wang, L.C., Zhu, J. and Huang, Q. (2017). Part II: $PM_{2.5}$ and polychlorinated dibenzo-*p*-dioxins and dibenzofurans (PCDD/Fs) in the ambient air of northern China. *Aerosol Air Qual. Res.* 17: 2010–2026.

Zhang, H. and Papadakis, G. (2010). Computational analysis of flow structure and particle deposition in a single asthmatic human airway bifurcation. *J. Biomech.* 43: 2453–2459.

Zhang, L., Asgharian, B. and Anjilvel, S. (1997). Inertial deposition of particles in the human upper airway bifurcations. *Aerosol Sci. Technol.* 26: 97–110.

Zhang, R., Liu, C., Hsu, P.C., Zhang, C., Liu, N., Zhang, J., Lee, H.R., Lu, Y., Qiu, Y. and Chu, S. (2016). Nanofiber air filters with high temperature stability for efficient $PM_{2.5}$ removal from the pollution sources. *Nano Lett.* 16: 3642–3649.

Zhang, Z., Kleinstreuer, C. and Kim, C. (2001). Flow structure and particle transport in a triple bifurcation airway model. *J. Fluids Eng.* 123: 320–330.

Zhang, Z., Kleinstreuer, C. and Kim, C. (2002). Gas–solid two-phase flow in a triple bifurcation lung airway model. *Int. J. Multiphase Flow* 28: 1021–1046.

Zheng, J., Hu, M., Peng, J., Wu, Z., Kumar, P., Li, M., Wang, Y. and Guo, S. (2016a). Spatial distributions and chemical properties of $PM_{2.5}$ based on 21 field campaigns at 17 sites in China. *Chemosphere* 159: 480–487.

Zheng, X., Xu, X., Yekeen, T.A., Zhang, Y., Chen, A., Kim, S.S., Dietrich, K.N., Ho, S.M., Lee, S.A. and Reponen, T. (2016b). Ambient air heavy metals in $PM_{2.5}$ and potential human health risk assessment in an informal electronic-waste recycling site of China. *Aerosol Air Qual. Res.* 16: 388–397.

Received for review, February 15, 2018
Revised, March 3, 2018
Accepted, March 8, 2018